Available online at www.sciencedirect.com
SCIENCE DIRECT®
Journal of Solid State Chemistry 177 (2004) 2726–2732
JOURNAL OF SOLID STATE CHEMISTRY
http://elsevier.com/locate/jssc

Crystal structures and phase transition in the system $SrTiO_3$–$La_{2/3}TiO_3$

Christopher J. Howard,[a,*] Gregory R. Lumpkin,[a,b] Ronald I. Smith,[c] and Zhaoming Zhang[a]

[a] *Australian Nuclear Science and Technology Organisation, Private Mail Bag 1, Menai NSW 2234, Australia*
[b] *Department of Earth Sciences, University of Cambridge, Downing Street, Cambridge CB2 3EQ, UK*
[c] *ISIS Facility, Rutherford Appleton Laboratory, Chilton, Didcot, Oxfordshire OX11 0QX, UK*

Received 28 February 2004; received in revised form 7 April 2004; accepted 8 April 2004

Abstract

The distribution of *A*-site cations in the perovskite system $La_xSr_{1-3x/2}TiO_3$ depends on the concentration of La^{3+} ions and associated vacancies. For small x ($x \lesssim 0.2$), the substitutions are expected to be random. For $x \geqslant 0.55$, the cations are ordered in such a way that successive layers of *A*-sites are occupied to greater and lesser degree, and this ordering drives a tetragonal distortion. For x from about 0.3 to 0.5, the X-ray patterns show diffuse peaks indicative of similar ordering, but this is not long-range order and no tetragonal distortion results. The lower temperature structures also exhibit out-of-phase tilting of the TiO_6 octahedra, setting in at temperatures varying linearly with composition from 105 K for $x = 0$, to about 650 K at $x = 2/3$.

Keywords: Perovskites; Cation/vacancy ordering; Synchrotron X-ray diffraction; Neutron powder diffraction

1. Introduction

The crystal structures and cation–vacancy ordering in perovskite systems with *A*-site vacancies are of interest for potentially attractive properties of ionic conductivity, dielectric behavior, and magnetic properties. Recently, it has been discovered that the system $SrTiO_3$–$La_{2/3}TiO_3$ also exhibits unusual behavior under external ion irradiation, with the critical temperature for amorphisation of $La_xSr_{1-3x/2}TiO_3$ showing a well-defined minimum at $x \approx 0.2$ [1]. We have undertaken X-ray and neutron powder diffraction studies of crystal structures and phase transitions in this system, with the particular aim of establishing the necessary structural basis for further interpretation and modelling of the radiation damage data. The studies also form part of our own systematic program of research on the structures and phase transitions in perovskites and related materials [2–7].

The structures of the $x = 0$ end member, $SrTiO_3$, are of course well known. At room temperature, $SrTiO_3$ is the perovskite aristotype, cubic, lattice parameter $a = 3.905$ Å, space group $Pm\bar{3}m$. Below about 105 K, $SrTiO_3$ adopts a tetragonal structure in space group $I4/mcm$. The tetragonal structure is characterised by the tilting of the corner-linked TiO_6 octahedra about their four-fold axes, the octahedra in successive layers being tilted in opposite senses. The tilt system is described in Glazer's notation [8,9] as $a^0a^0c^-$, this indicating out-of-phase (-) tilting around the [001]-axis of the perovskite aristotype. It is worth noting, for purposes of later discussion, that the tilt axis could equally well be taken to lie along the parent [100], in which case the Glazer symbol would read $a^-b^0b^0$. This 105 K transition is a soft mode transition and a text book classic [10]. The transition temperature has been recently redetermined, in a low temperature calorimetric study [11], as 105.7 K.

It is only recently that the structures at the La rich end, near $x = \frac{2}{3}$, have been fully understood. The most notable feature of these structures is a layered ordering of La^{3+} cations onto the perovskite *A*-sites, such that one layer of *A*-sites is essentially fully occupied by La^{3+} cations, and the next layer is only about $\frac{1}{3}$ occupied. This cation–vacancy ordering reduces the symmetry to

*Corresponding author. Fax: +61-9543-7179.
E-mail address: cjh@ansto.gov.au (C.J. Howard).

0022-4596/$ - see front matter © 2004 Elsevier Inc. All rights reserved.
doi:10.1016/j.jssc.2004.04.018

tetragonal, and leads to a doubling of the c-parameter (relative to that in the parent perovskite). The space group is $P4/mmm$. This structure is observed, however, only at temperatures above about 650 K. The room temperature structure in fact shows an orthorhombic distortion. It has only been recognised in the last 2 years [12–14] that this orthorhombic distortion is a consequence of octahedral tilting in this material. The high temperature structure can be described, in Glazer notation, as $a^0a^0c^0$, where the c is used to distinguish the direction normal to the layers developed in the cation–vacancy ordering, and the superscripts are '0' because there is no octahedral tilting. The octahedral tilting in the room temperature structure is about an axis perpendicular to this direction, the tilt system is accordingly described in Glazer notation as $a^-b^0c^0$. The structure is described in space group $Cmmm$, on a cell doubled (relative to the parent perovskite) along each of its axes. The reader is referred to our previous work [7,14] for detail.

There have been previous studies on the system $La_xSr_{1-3x/2}TiO_3$, reporting somewhat conflicting results [15–18]. Our current understanding of the situation, as will be elaborated in the later section, is as follows. The samples are prepared at temperatures in excess of 1300°C, and then usually furnace cooled. The cation distribution is established at temperatures above about 1000°C, this estimate being based on the suggestion, from high temperature X-ray studies [19], that cations are mobile only above this temperature. The cation distributions may be sensitive to the rate of cooling through 1000°C [18]. We expect that cations and vacancies will be randomly distributed for low values of x ($x \lesssim 0.2$), and may show short-range order for higher values of x ($0.3 \lesssim x \lesssim 0.5$). We have established [14] that they exhibit long-range order leading to tetragonal distortion for the highest values of x ($x > 0.5$). The structures are (in the absence of octahedral tilting) cubic in $Pm\bar{3}m$, Glazer symbol $a^0a^0a^0$, in the absence of long-range A-site cation ordering, and tetragonal in $P4/mmm$, $a^0a^0c^0$, once long-range order is established. Evidently, these structures are subject to a transition in which lowering of the temperature sees the onset of octahedral tilting, about one axis of the parent perovskite. Structures initially cubic become tetragonal, in space group $I4/mcm$, $a^-b^0b^0$, and those initially tetragonal become orthorhombic, in space group $Cmmm$, $a^-b^0c^0$. The four pertinent structures are illustrated in Fig. 1. The primary aim in this work was to determine at what compositions the cation–vacancy distribution showed random, short- and long-range order, and to determine for each composition the onset temperature for the octahedral tilting. The influence, if any, of short- or long-range cation–vacancy order on octahedral tilting transition temperatures, and tilt angles, should become apparent.

2. Experimental and data analysis

Samples of $La_xSr_{1-3x/2}TiO_3$ at $x = 0.1$, 0.2, 0.3, 0.4, 0.45, 0.5, 0.55, 0.6, 0.67 were produced by the standard alkoxide/nitrate route [20]. Stoichiometric quantities of ethanolic titanium isopropoxide were first hydrolysed by mixed lanthanum/strontium nitrate aqueous solutions. After mixing and stir drying, the materials were calcined in air at 750°C for 1 h to remove nitrates and alcohol, then wet milled for 16 h using zirconia balls. Each slurry was then dried at 110°C overnight, and the dried clumps were ground in a mortar and pestle into fine powder. The powders were pressed into 10 g pellets, sintered in air at 1500°C for 48 h, then cooled in the furnace, to 1100°C at 300°C h^{-1}, slow cooled at 3°C h^{-1} from 1100°C to 500°C, and furnace cooled to room temperature. Samples were analyzed using a JEOL 6400 scanning electron microscope fitted with an energy dispersive spectrometer. This verified sample compositions, and showed samples up to $x = 0.6$ to be homogeneous solid solutions, with trace amounts of rutile in some samples. The sample at $x = 0.67$ was evidently not single phase, and no further studies were made on this. The $x = 0$ end member, $SrTiO_3$, was a powder sample (325 mesh), supplied by Electronic Space Products International, Oregon, USA.

X-ray diffraction patterns were recorded using the Australian National Beamline Facility's powder diffractometer [21], located on beamline 20B at the Photon Factory, KEK, Japan. The instrument is a 573 mm (radius) Debye–Scherrer camera, the data being recorded on image plates. The X-ray wavelength was $\lambda = 0.79$ Å. Further details on experimental procedures, the furnace used for the high temperature work, and the analysis of the X-ray patterns have been given in our earlier paper [14].

Time-of-flight powder neutron diffraction patterns were recorded using the instrument Polaris [22] at the ISIS neutron facility, Rutherford-Appleton Laboratory, UK. The samples, either $SrTiO_3$ powder, or for samples at $x \neq 0$ broken pieces of pellet, were loaded into thin-walled 11 mm diameter vanadium sample cans (Metal Technology Inc., Albany, OR, USA) which were then mounted according to requirement. For measurements at room temperature the cans were suspended from the standard ISIS candlesticks. For measurements below room temperature they were loaded into an Oxford Variox cryostat, or an AS Scientific, 50 mm diameter, 'Orange' cryostat, helium exchange gas being introduced into the sample chamber to a pressure of ~40 mbar. Temperature was monitored using two Rh/Fe sensors, one mounted on the cryostat heat exchanger and the other on the sample stick. For measurements above room temperature the samples were loaded into an ISIS designed 1000°C furnace (RAL F2) which employs a cylindrical vanadium element and operates under high

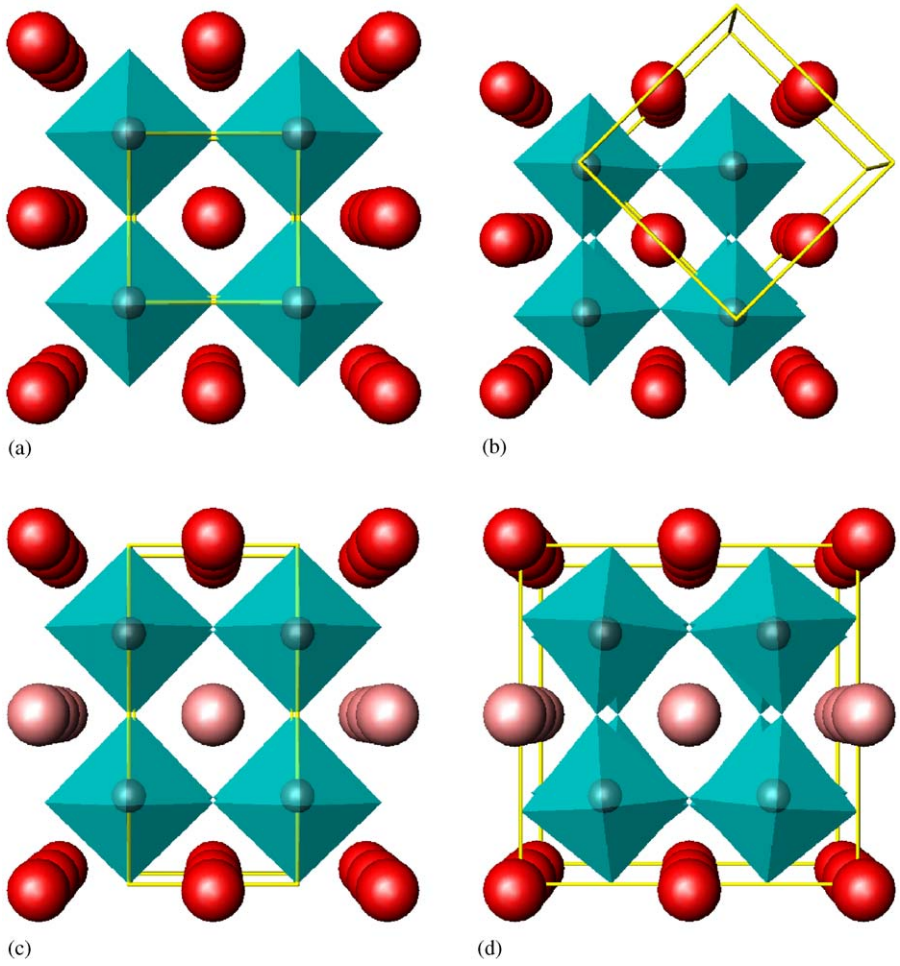

Fig. 1. Perspective views, along the x-axis, of structures encountered in the system $La_xSr_{1-3x/2}TiO_3$. The TiO_6 are shown as octahedra. The spheres outside these octahedra represent the La/Sr ions; the darker and lighter spheres in the structures in the lower diagram representing layers with greater and lesser occupancy as occur in the ordered structures. Octahedral tilting, about the x-axis, can be seen in the structures shown at the right. The unit cell is outlined in each case. These figures were prepared using ATOMS version 5.0.7, ©Eric Dowty, 1999: (a) $Pm\bar{3}m(a^0a^0a^0)$ (b) $I4/mcm(a^-b^0b^0)$ (c) $P4/mmm(a^0a^0c^0)$ (d) $Cmmm(a^-b^0c^0)$.

vacuum (pressure $<10^{-4}$ mbar). Temperatures were monitored and controlled using two type K thermocouples, one located close to the furnace element, the other mounted on the sample stick and placed in contact with the sample can. Diffraction data were recorded in all of the Polaris detectors, with the data from the 145° bank (recording d-spacings from 0.3 to 3.2 at a resolution $\Delta d/d \sim 5 \times 10^{-3}$) and the 90° bank (from 0.4 to 4 Å at $\Delta d/d \sim 7 \times 10^{-3}$) used in the subsequent analysis. First, the time-of-flight data from the individual detector elements comprising a particular detector bank were converted to d-spacing and summed, to produce a single pattern from that bank. Then, after subtracting an instrumental background, the patterns were normalised by dividing by a spectrum derived from the measurement of incoherent scattering from a vanadium rod (to account for the variation with neutron wavelength of both the incident flux and the detector efficiency). All data were recorded to a minimum total incident proton beam of 85 μA h, corresponding to about 30 min beamtime.

An important first step in any data analysis is inspection of the diffraction patterns, with a view to identifying the structures obtained. The main perovskite peaks were inspected for broadening or splitting, which would indicate a tetragonal distortion accompanying cation ordering and/or octahedral tilting. In addition, a search was made for superlattice peaks, particularly at the X-point (one index half-integral when referred to the cell of the parent perovskite) where the layered ordering of cations would be seen, and at the R-point (all indices half-integral) where peaks from out-of-phase octahedral tilting should be seen. Peak splitting should be more evident in the X-ray patterns, by virtue of the higher resolution in these patterns, and X-rays should also show the cation ordering effects. On the other hand, octahedral tilting involves movement of the oxygen ions only, so it is anticipated that the R-point reflections will

show more strongly in the neutron patterns than in the X-ray ones. Pertinent aspects of the data processing will be explained as required below.

3. Results and discussion

3.1. Room temperature studies

3.1.1. X-ray diffraction

In contrast with our earlier X-ray study [14] of a single composition ($x = 0.6$) at different temperatures, the focus here will be on the room temperature X-ray patterns recorded from samples of different compositions. Patterns from the different samples as recorded on the first image plate ($5 < 2\theta < 45°$) are shown in Fig. 2. The pattern at composition $x = 0.6$ is very similar to that shown in our previous report [14]. The main perovskite peaks are indexed on the basis of the aristotype cubic ($1 \times 1 \times 1$) cell. The various superlattice peaks are labelled *X*- or *R*-point reflections according as they index on this cell with one or all half-integral indices. At the *X*-points, broad features indicative of short-range cation/vacancy ordering become quite evident at $x = 0.4$ (with indications of analogous features also at $x = 0.3$), and these become sharper and more intense as the La content (x) increases. In our previous study [14], we concluded that long-range cation/vacancy ordering is established at $x = 0.6$, and that this long-range ordering gives rise to a tetragonal distortion. Examining the main perovskite peaks, we see no indication of splitting or broadening up to $x = 0.5$, so we conclude that for $x \leqslant 0.5$ there is no tetragonal distortion and no long-range cation/vacancy ordering.[1] At $x = 0.55$, however, the main peaks are split or broadened, indicating the onset at this composition of long-range order and the concomitant distortion. The *R*-point reflections, associated with TiO_6 octahedral tilting, are much weaker features, as is expected in the X-ray case. They are, however, still quite discernible from $x = 0.3$ (Fig. 2b), with still perhaps some very weak indication of *R*-point intensity at $x = 0.2$.

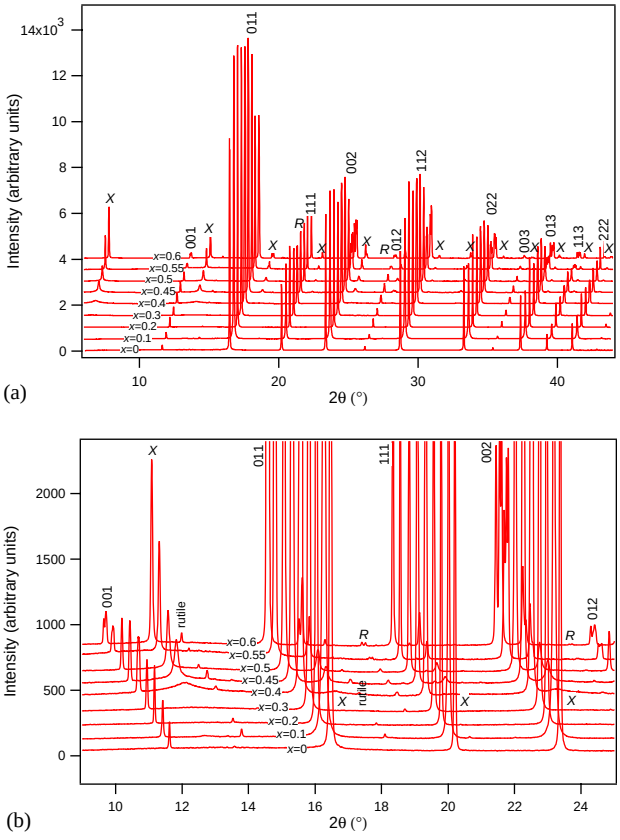

Fig. 2. (a) X-ray diffraction patterns, as recorded on the first image plate ($5 < 2\theta < 45°$), from samples of $La_xSr_{1-3x/2}TiO_3$ at room temperature. The main peaks have been indexed on the basic perovskite cell. Superlattice peaks at the *X*- and *R*-points arise from cation/vacancy ordering on the perovskite *A*-sites, and tilting of the TiO_6 octahedra, respectively. No splitting or broadening of the main perovskite peaks is evident up to (and including) $x = 0.5$. (b) The same patterns on horizontally and vertically expanded scales. The *R*-point reflections, though very weak, are discernible at $x = 0.3$ and above. Features at the *X*-points, though initially broad, are quite apparent at $x = 0.4$ and above. Peaks attributable to a small quantity of TiO_2 (rutile) impurity can also be seen.

Although we have not undertaken any detailed (Rietveld) analysis of the X-ray diffraction patterns, the composition dependence of intensity and width of the *X*-point reflections merits further comment. We focus attention on the *X*-point reflection at $2\theta = 13.1°$. At compositions $x = 0.6$ and 0.55, this has width (full-width at half-maximum) $\sim 0.06°$, and is only marginally wider than the main 1 1 1 peak, which remains a single peak for all the structures considered. This is consistent with the long-range cation ordering found at these compositions. This peak is broader for lower values of x, increasing in width from $\sim 0.09°$ at $x = 0.5$, through $\sim 0.14°$ at $x = 0.45$, to $\sim 0.95°$ at $x = 0.4$. Making use of the Scherrer equation [23]:

$$t = \frac{0.9\lambda}{B\cos\theta},$$

where B is the full-width at half-maximum (in radian, after allowing for instrumental contributions) of a reflection appearing at angle 2θ, we estimate the range t of the cation ordering as ~ 100 nm at $x = 0.5$, through ~ 50 nm at $x = 0.45$, down to ~ 5 nm at $x = 0.4$. The intensity of this reflection, measuring the difference in scattering power between successive layers of *A*-sites, also falls as the La content x diminishes.

[1] This means of distinguishing short- from long-range cation ordering is admittedly somewhat arbitrary. Additional evidence comes from the fact that, at compositions $x \leqslant 0.5$, the peaks appearing at the *X*-points remain significantly broader than the main perovskite peaks, hence the domains of cation ordering are significantly smaller in size than the crystallites.

3.1.2. Neutron diffraction

Shown in Fig. 3 are extracts ($0.8 < d < 2.8$ Å) from the neutron diffraction patterns recorded in the Polaris 145° detector bank from samples of different compositions. The peaks are marked as in the X-ray patterns, though since d-spacing decreases as 2θ increases, the peaks appear in the reverse order. The R-point reflections are evident from $x = 0.3$, with perhaps again a very weak indication of these reflections at $x = 0.2$. The X-point reflections are relatively weaker in the neutron patterns than the X-ray ones, but can be seen nevertheless from about $x = 0.45$. The resolution in the neutron patterns, $\Delta d/d \sim 5 \times 10^{-3}$, is a little inferior to that in the X-ray patterns (reckoned at $\Delta d/d \sim 3.5 \times 10^{-3}$ for the 1 1 1 reflection), so the neutron patterns are less informative on matters such as splitting of the main peaks due to orthorhombic distortion, or broadening of the X-point features as a consequence of the short-range nature of cation/vacancy ordering.

These neutron diffraction patterns were fitted over the range $0.4 < d < 3.2$ Å using the Rietveld method, as implemented in the GSAS computer program [24].

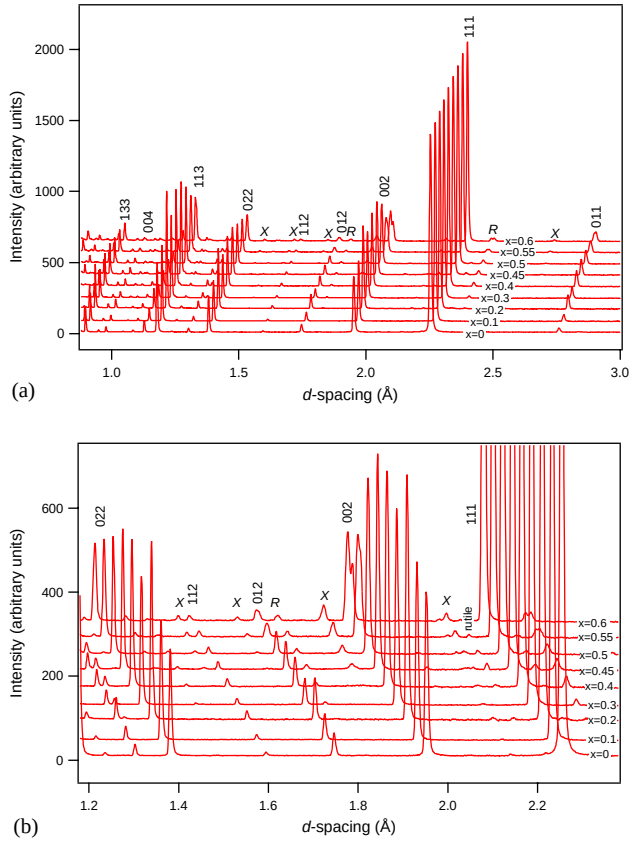

Fig. 3. (a) Extracts from the neutron diffraction patterns, as recorded by Polaris in the 145° detector bank, from samples of $La_xSr_{1-3x/2}TiO_3$ at room temperature. The peaks are marked as in the X-ray patterns, though it may be noted that relative to that pattern their order is reversed. (b) The same patterns on horizontally and vertically expanded scales.

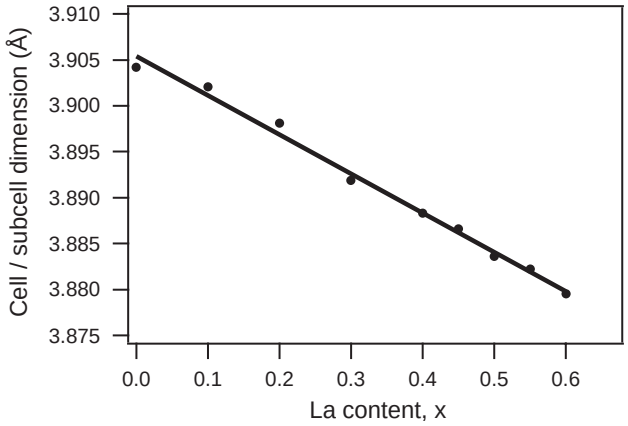

Fig. 4. Cubic lattice parameter or perovskite subcell dimension, from samples of $La_xSr_{1-3x/2}TiO_3$ at room temperature. These results are from Rietveld method analysis of the neutron diffraction patterns—analysis of X-ray patterns gave comparable results.

Based on the inspection of X-ray and neutron patterns just discussed, we identified the structures as being cubic in $Pm\bar{3}m$ for $x = 0, 0.1$, cubic or possibly $I4/mcm$ tetragonal for $x = 0.2$, tetragonal in $I4/mcm$ for $x = 0.3$, 0.4, 0.45, 0.5, and orthorhombic in $Cmmm$ for $x = 0.55$, 0.6. The peak shapes in the neutron patterns were modelled as convolutions of exponential with pseudo-Voigt [24] in which two peak width parameters were varied, and the background with eight-parameter shifted Chebyshev polynomials. An extinction parameter and isotropic atomic displacement parameters were also refined. We have obtained from this analysis values for the lattice parameters, and for the atomic co-ordinates.

As regards the lattice parameters, we present in Fig. 4 values of the lattice parameter a for the cubic structure, and for the other structures the cube root of an appropriately reduced unit cell volume, corresponding to the edge of the basic perovskite subcell. Evidently, the subcell dimension decreases approximately linearly with La content. This result is confirmed by examining X-ray peak positions, but the X-ray results show more scatter despite the higher resolution, presumably because the different patterns were measured on different runs and on different occasions.

From the atomic co-ordinates we estimate the angle of tilt ϕ of the octahedra. This angle is of course zero in the $Pm\bar{3}m$ structure, is obtained using $\phi = \tan^{-1}4(x(\mathrm{O2}) - \frac{1}{4})$ for tetragonal $I4/mcm$ [25], and from $\phi = \tan^{-1}2(y(\mathrm{O1}) - y(\mathrm{O2}))$ in orthorhombic $Cmmm$ [14]. The tilt angle increases with La content, ranging from perhaps $\sim 1°$ at $x = 0.2$, through 3.2° at $x = 0.5$, to 4.6° at $x = 0.6$. There is some evidence of a step increase in tilt angle at the boundary between structures in $I4/mcm$ (no long-range cation/vacancy ordering) and those in $Cmmm$ (long-range ordering), but a more detailed study would be necessary to establish this step increase beyond doubt.

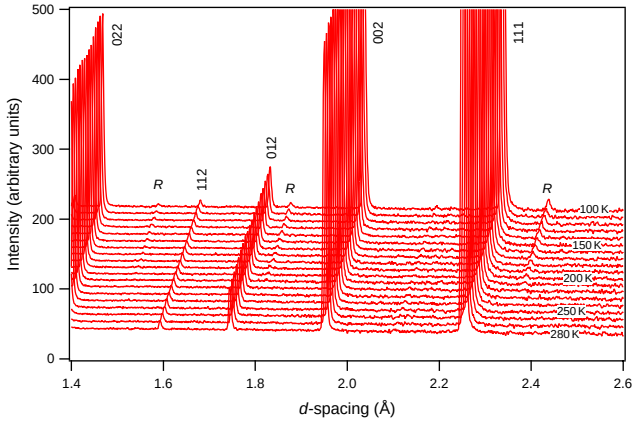

Fig. 5. Extracts from the neutron diffraction patterns, as recorded in the Polaris 145° detector bank, from the sample of $La_{0.1}Sr_{0.85}TiO_3$ at different temperatures. The temperatures range from 100 K (at back) in steps of 10 to 280 K (at front). The first signs of the *R*-point reflections appear at about 210 K, which is taken to be the temperature of the octahedral tilting transition.

3.2. Variable temperature studies

The purpose of the variable temperature studies was to determine, for each composition, the transition temperature marking the onset (or disappearance upon heating) of octahedral tilting. For the $x = 0$ end member, this has been determined in a precise calorimetric study [11] as 105.7 K. In our previous X-ray study, at composition $x = 0.6$, we estimated the transition temperature at 633 K. Determination of the transition temperatures by diffraction methods depends on monitoring or measuring the *R*-point reflections. Since, as previously mentioned, these are relatively stronger in the neutron patterns than the X-ray patterns, neutron methods were preferred for this work.

Neutron diffraction patterns were therefore recorded from each sample at a number of temperatures, the temperature range being selected according to the transition temperature expected. By way of example, patterns were recorded from the $x = 0.1$ sample, $La_{0.1}Sr_{0.85}TiO_3$, in the Oxford Variox cryostat, at temperatures from 100 K in 10 K steps to 280 K. Extracts from these diffraction patterns are shown in Fig. 5. By inspection, the first signs of the *R*-point reflections are seen at about 210 K, and we take this to be the transition temperature required.[2]

A similar approach was taken at other compositions, though for $x \geqslant 0.3$, measurements above room temperature were appropriate. The results for the temperatures of the octahedral tilting transition are included in Fig. 6,

[2] An alternative approach would be to use refined atomic coordinates to estimate tilt angle ϕ, and to extrapolate on the assumption this is the order parameter for a continuous second-order transition. This is equivalent to the approach we used in our earlier work on $La_{0.6}Sr_{0.1}TiO_3$ [14], and gives a higher value for the transition temperature, but we are now less certain of its validity.

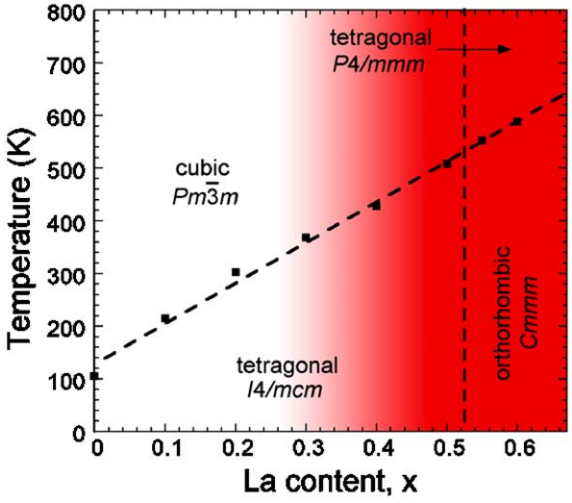

Fig. 6. A summary of the results on $La_xSr_{1-3x/2}TiO_3$. The shading indicates the degree of cation/vacancy ordering: random to $x \approx 0.2$, then short-range, and finally long-range for $x \geqslant 0.55$ (but see footnote 1). The points mark the observed temperatures of the octahedral tilting transition, and the sloping dashed line is a fit through these points. The structures resulting from the different combinations of cation/vacancy ordering and octahedral tilting are indicated on the plot.

Section 4, where it will be seen that the octahedral tilting transition temperature varies practically linearly with composition.

3.3. A measurement at low temperature

There has been some discussion of the possibility of additional low temperature phases occurring in $SrTiO_3$ [26], but no diffraction evidence for such phases has been found [27]. It was also considered prudent (A.M. Glazer, personal communication) to check for any additional phases occurring at the La rich compositions, and to this end we recorded a pattern from $La_{0.6}Sr_{0.1}TiO_3$ at 2 K. The diffraction pattern is exceedingly well fitted assuming the same *Cmmm* structure as occurs at higher temperature, with lattice parameters $a = 7.7493(1)$ Å, $b = 7.7179(1)$ Å, $c = 7.7729(1)$ Å (effective subcell dimension reduced to 3.8733 Å), and octahedral tilt angle increased to 5.5°.

4. Summary and conclusions

Compositions across the system $La_xSr_{1-3x/2}TiO_3$ have been studied using both synchrotron X-ray and neutron powder diffraction techniques, at room temperature and at variable temperature below or above room temperature as appropriate. The main conclusions have been incorporated into the schematic Fig. 6.

Structures in the system as prepared for this work are characterised by a layered cation/vacancy ordering on the perovskite *A*-sites, and by octahedral tilting.

The cation/vacancy ordering is evidenced by the presence of peaks (X-point) indexing on the basic perovskite subcell with just one half-integral index. These peaks are sharp, indicative of long-range order for $x>0.5$ and a significant tetragonal distortion is associated with this effect. The boundary indicating the onset of long-range order is included on the schematic. The same X-point reflections are present for $0.3\lesssim x\lesssim 0.5$, but broader and less intense, suggesting the occurrence of short-range order in samples in this composition range.

Octahedral tilting is best studied by monitoring peaks (R-point) with all indices half-integral, when related to the same perovskite subcell, and these are best followed by neutron diffraction. So neutron diffraction patterns were recorded at each composition as a function of temperature, in order to estimate the temperatures of disappearance (upon heating) or onset (upon cooling) of octahedral tilting. A plot of this transition temperature, against composition, is also included on the schematic.

The transition temperature for octahedral tilting varies practically linearly with composition, there being no evidence of any major influence on this temperature of the nature (short- or long-range) of the cation/vacancy ordering established.

It can be seen, from the schematic, that room temperature (300 K) structures are cubic to $x\approx 0.2$, tetragonal in $I4/mcm$ to $x=0.5$, then orthorhombic in $Cmmm$ from $x=0.55$. Structures in $I4/mcm$, while undoubtedly having tetragonal symmetry consequent upon the octahedral tilting, were found to be metrically cubic to the resolution of our work. A more detailed analysis of the neutron patterns revealed an increase in the octahedral tilt angle with increasing x, with the suggestion that this increases stepwise when long-range cation/vacancy ordering sets in. Further work would be required to confirm this behavior. It is not clear to us that these structural results will lead to any better understanding of the amorphisation resistance in these materials, though we do note that the resistance to amorphisation is greatest at compositions around $x=0.2$, which is also a composition at which the octahedral tilting transition takes place at room temperature.

Acknowledgments

The authors gratefully acknowledge the assistance of Ms. Mugdha Bhati, ANSTO, in making the samples. Dr. James Hester provided, during the conduct of the X-ray measurements, valuable advice and support. The neutron facilities at ISIS are operated by the Council for the Central Laboratory of the Research Councils (CCLRC), with a contribution from the Australian Research Council. Travel funding to ISIS was provided by the Access to Major Research Facilities Program. The X-ray measurements were performed at the Australian National Beamline Facility with support from the Australian Synchrotron Research Program, which is funded by the Commonwealth of Australia under the Major National Research Facilities Program.

References

[1] K.L. Smith, G.R. Lumpkin, M.G. Blackford, E.R. Vance, Mater. Res. Symp. Proc. 540 (1999) 323–329.
[2] C.J. Howard, H.T. Stokes, Acta Crystallogr. B54 (1998) 782–789 (Erratum, Acta Crystallogr. B58 (2002) 565).
[3] C.J. Howard, K.S. Knight, B.J. Kennedy, E.H. Kisi, J. Phys.: Condens. Matter 12 (2000) L677–683.
[4] C.J. Howard, V. Luca, K.S. Knight, J. Phys.: Condens. Matter 14 (2002) 377–387.
[5] H.T. Stokes, E.H. Kisi, D.M. Hatch, C.J. Howard, Acta Crystallogr. B 58 (2002) 934–938.
[6] C.J. Howard, B.J. Kennedy, P.M. Woodward, Acta Crystallogr. B 59 (2003) 463–471.
[7] C.J. Howard, Z. Zhang, Acta Crystallogr. B 60 (2004) 249–251.
[8] A.M. Glazer, Acta Crystallogr. B 28 (1972) 3384–3392.
[9] A.M. Glazer, Acta Crystallogr. A 31 (1975) 756–762.
[10] H.D. Megaw, Crystal Structures—A Working Approach, W.B. Saunders, Philadelphia, 1973, pp. 464–466.
[11] E.K.H. Salje, M.C. Gallardo, J. Jirnénez, F.J. Romero, J. del Cerro, J. Phys.: Condens. Matter 10 (1998) 5535–5543.
[12] Y. Inaguma, T. Katsmata, M. Itoh, Y. Morii, J. Solid State Chem. 166 (2002) 67–72.
[13] M. Yashima, M. Mori, T. Kamiyama, K. Oikawa, A. Hoshikawa, S. Torii, K. Saitoh, K. Tsuda, Chem. Phys. Lett. 375 (2003) 240–246.
[14] C.J. Howard, Z. Zhang, J. Phys.: Condens. Matter 15 (2003) 4543–4553.
[15] T.Y. Tien, F.A. Hummel, Trans. Br. Ceram. Soc. 66 (1969) 233–245.
[16] J. Bouwma, K.J. de Vries, A.J. Burggraaf, Phys. Status Solidi A 35 (1976) 281–289.
[17] U. Balachandran, N.G. Eror, J. Am. Ceram. Soc. 64 (1981) C75–C76.
[18] P.D. Battle, J.E. Bennett, J. Slan, R.J.D. Tilley, J.F. Vente, J. Solid State Chem. 149 (2000) 360–369.
[19] M. Yashima, R. Ali, H. Yoshioka, Solid State Ion. 128 (2000) 105–110.
[20] A.E. Ringwood, S.E. Kesson, K.D. Reeve, D.M. Levins, E.J. Ramm, in: W. Lutze, R.C. Ewing (Ed.), Radioactive Waste Forms for the Future, Elsevier, Amsterdam, 1988, pp. 233–334.
[21] T.M. Sabine, B.J. Kennedy, R.F. Garrett, G.J. Foran, D.J. Cookson, J. Appl. Crystallogr. 28 (1995) 513–517 (see also http://www.ansto.gov.au/natfac/asrp1.html).
[22] R.I. Smith, S. Hull, A.R. Armstrong, Mater. Sci. Forum 166–169 (1994) 251–256 (see also http://www.isis.rl.ac.uk/crystallography/polaris).
[23] B.D. Cullity, Elements of X-ray Diffraction, Addison-Wesley, Reading, MA, 1978, p. 102.
[24] A.C. Larson, R.B. Von Dreele, General structure analysis system (GSAS), Report LAUR 86-748, Los Alamos National Laboratory, 1994.
[25] B.J. Kennedy, C.J. Howard, B.C. Chakoumakos, Phys. Rev. B 59 (1999) 4023–4027 (see also R.H. Mitchell, Perovskites Modern and Ancient, Almaz Press, Thunder Bay, Ont., 2002, p. 23).
[26] K.A. Muller, W. Berlinger, E. Tosatti, Z. Phys. B 84 (1991) 277–283.
[27] J.M. Kiat, T. Roisnel, J. Phys.: Condens. Matter 8 (1996) 3471–3475.